Desalination and Water Treatment
www.deswater.com

doi: 10.5004/dwt.2020.26014

198 (2020) 386–395
September

Acacia nilotica for adsorption of Bismarck Brown Y and Reactive Black 5 dyes in batch reactors: isotherm models and kinetics studies

Muhammad Tahir Amin[a,b,*], A.A. Alazba[a,c], Muhammad Shafiq[a]

[a]*Alamoudi Water Research Chair, King Saud University, P.O. Box: 2460, Riyadh 11451, Saudi Arabia, Tel. +966114673737; Fax: +966114673739; emails: mtamin@ksu.edu.sa (M.T. Amin), alazba@ksu.edu.sa (A.A. Alazba), msrana@ksu.edu.sa (M. Shafiq)*
[b]*Department of Environmental Sciences, COMSATS University Islamabad, Abbottabad Campus, Pakistan*
[c]*Agricultural Engineering Department, King Saud University, P.O. Box: 2460: Riyadh 11451, Saudi Arabia*

Received 12 September 2019; Accepted 20 April 2020

ABSTRACT

Acacia nilotica (AN) was found to be an effective adsorbent for removing Bismarck Brown Y (BBY) and Reactive Black 5 (RB5) dyes from aqueous solutions in a batch reactor. Scanning electron microscopy and energy dispersive X-ray analysis of the AN adsorbent were performed to study its morphology and elemental composition, respectively. The maximum adsorption capacity of the AN adsorbent for the RB5 and BBY dyes was determined to be 38.38 and 39.31 mg/g in 120 and 30 min, respectively. The adsorption capacity of the AN adsorbent increased from 7.37 to 104.79 mg/g for the RB5 dye and from 19.65 to 113.48 mg/g for the BBY dye as the dye concentration in the solution increased from 25 to 180 mg/L. The maximum adsorption capacities of the AN adsorbent for the RB5 and BBY dyes at a pH of 2 were 19 and 40.07 mg/g, respectively. Pseudo-first-order kinetic model fitted the adsorption data for initial 30 min of contact time and pseudo-second-order kinetics fitted the adsorption data well (coefficient of determination = 0.94–0.96) expressing the chemical adsorption. Langmuir isotherm model adequately fitted the adsorption data of both dyes suggesting the predominant monolayer adsorption.

Keywords: Batch adsorption; Dye concentration; Isotherm behavior; Pseudo-second-order kinetics

1. Introduction

The concept of sustainable development has made it obligatory for solid waste management plants to either convert waste into useful products or undertake sequestration of hazardous pollutants from aqueous solutions [1]. This integrated management strategy is beneficial because of the procurement of potentially useful products from waste and the restoration of the quality of water streams [2]. The continuous depletion of natural resources in terms of quality and quantity has necessitated the development of sustainable technologies [3] and an urgent search for suitable methods to treat industrial effluents released by complex textile units. These steps can assure the restoration of water quality and render water bodies, which receive the untreated wastewater discharge of textile industries, reusable [4].

The toxicity, mutagenicity, and carcinogenicity of reactive dyes are primarily because of the presence of the azo (–N=N–) group [5–7]. Moreover, dye colors in water bodies reduce the penetration of light and interrupt the process of photosynthesis, adversely affecting the aquatic ecosystem [8]. These toxic dyes may result in dermatitis, skin irritation, allergy, bladder cancer, genotoxicity, and mutations

* Corresponding author.

when they come in contact with human bodies [9,10]. In view of these hazards, it is necessary to seek economical alternatives to remove hazardous pollutants from textile effluents prior to their discharge into freshwater bodies.

Most traditional methods of decolorization, including coagulation and flocculation [11,12], electrochemical methods [13], removal by activated carbon [14], use of polymeric adsorbents [14], mineral bentonite clays [15], membrane filtration [16], nanofiltration [17], chemical oxidation [18], ion exchange [19], and degradation [20], can separate reactive dye pollutants from aqueous solutions and/or wastewater to a certain extent. However, most of these methods are incapable of removing reactive dyes owing to the complex polyaromatic structures and recalcitrance of reactive dyestuffs [21]. Moreover, the application and effectiveness of these particular methods may be restricted as a result of the complex composition of textile wastewater, especially when it is loaded with various types of dyes, salts, and metals in variable concentrations [22].

Timber waste has recently attracted the attention of the scientific community for the sorption of dyes owing to its low cost and applicability for the removal of various types of dyes. To date, numerous studies have been reported in the literature on the methods available with various removal potentials for the sorption of different types of dyes. For instance, boron industry waste and *Melia azedarach* sawdust were utilized for the removal of anionic dyes [23]. Rosewood sawdust and industrial wastes were used for the sequestration of basic dyes [24,25]. Agricultural wastes were utilized for cationic and anionic dyes [26]. Activated carbon from sugarcane bagasse and agricultural wastes were used in the treatment of reactive dyes [27,28]. Eucalyptus bark and sugarcane bagasse were employed for direct dye treatment [29]. In the present study, the potential of the *Acacia nilotica* (AN) was investigated as an adsorbent for the treatment of Reactive Black 5 (RB5) and Bismarck Brown Y (BBY) dyes in a batch reactor. Furthermore, the various parameters influencing dye adsorption were optimized, and the adsorption mechanism of the AN adsorbent was explained using isotherms and fit of kinetics models.

2. Experimental

Analytical (Merck, Germany) grade RB5 ($C_{26}H_{21}N_5Na_4O_{19}S_6$, molecular weight: 991.82 g/mol) and BBY ($C_{18}H_{18}N_8$, molecular weight: 419.31 g/mol) (Fig. 1) dyes were chosen as the model contaminants in this study. Their respective molecular weights are 991.82 and 419.31 g/mol. Their stock solutions in concentrations of 1,000 mg/L (1,000 ppm) were prepared using distilled water and the working solutions were prepared by diluting the stock solutions.

2.1. Collection and preparation of timber waste

AN was selected as the source of timber waste biomass. The AN waste biomass was collected from the local wood industry in the Kingdom of Saudi Arabia. The adsorbent was washed with distilled water, dried, chopped into small pieces, and ground. The waste biomass was then sieved and the required mesh size (40 mesh, 400 μm) was chosen for the batch reactor studies.

2.2. Surface characterization

Scanning electron microscopy (SEM, HITACHI S-3000N, JAPAN) was conducted to study the surface morphology and texture of the AN waste biomass before the loading of the RB5 and BBY dyes. The SEM micrographs were obtained at magnifications of ×250, ×500, and ×2,000 before the treatment of the RB5 and BBY dyes from their aqueous solutions, and the visibly porous nature of the AN surface was analyzed. An acceleration voltage of 5 kV and a working distance of 25 mm were maintained for the measurements. Dry powder samples were fixed on a specified SEM steel stab holder with the help of double edge carbon tape. Afterward, stabs along with powder samples were coated with a thin layer of platinum (platinum coater device under vacuum condition) to avoid electrostatic charging of the samples. After platinum coating, steel stab holders were inserted to the SEM sample chamber to take the images under a high vacuum. Energy dispersive X-ray (EDX) analysis was additionally performed to determine the elemental composition of the AN waste adsorbent. Fourier transform infrared (FTIR) spectroscopy was performed using the Vertex-70 instrument (Bruker, USA) to analyze the functional groups present on the adsorbent surface before and after the removal of the dyes. Attenuated total reflectance method was used in FTIR spectroscopy to determine surface properties of solid material with a resolution of 4 cm^{-1}, the spectral range of 600–4,000 cm^{-1} and 16 number of sample scans.

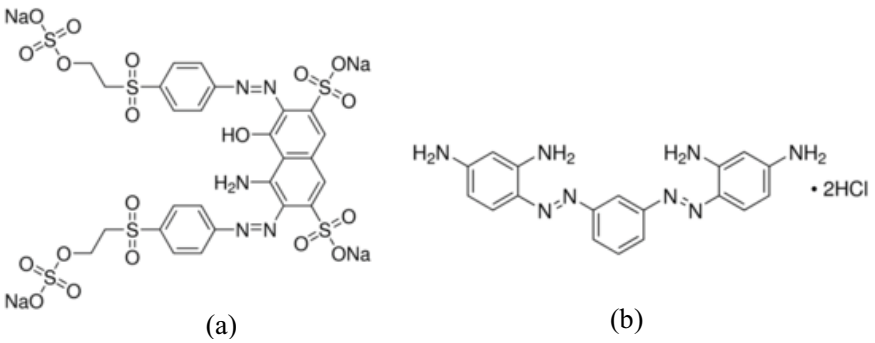

Fig. 1. Chemical structures of RB5 dye (a) and BBY dye (b).

2.3. Batch reactor studies

Batch adsorption studies were conducted in 100 mL Erlenmeyer flasks. Fixed amounts of the AN waste adsorbent (0.05 g) and the BBY and RB5 dyes, that is, 50 mg/L (50 mL solution volume), were added separately. The particle size of AN was approximately 420 μm (in the range 20–40 mesh, i.e., 420–841 μm), and this was maintained constant. Moreover, a mesh size of 40 (420 μm) was chosen for the batch experiments. The flasks were placed in a temperature-controlled shaking incubator and agitated at 220 rpm and 30°C. The samples were withdrawn from the flasks and the residual concentrations of RB5 and BBY in the filtrate were measured at 698 and 457 nm, respectively, using a double beam ultraviolet/visible light (UV/Vis) spectrophotometer (T80+, PG Instruments, UK). The adsorption capacities of the AN waste adsorbent (q, mg/g) at time t and equilibrium (q_e, mg/g) were calculated using Eqs. (1) and (2), respectively. The removal efficiencies (sorption percentages) of the dyes from the solution phase were calculated using Eq. (3).

$$q_t = \left(\frac{C_0 - C_t}{m}\right)V \tag{1}$$

$$q_e = \left(\frac{C_0 - C_e}{m}\right)V \tag{2}$$

$$\text{Removal}(\%) = \frac{(C_0 - C_e)}{C_0} \times 100 \tag{3}$$

Here C_0, C_t, and C_e (mg/L) refer to the solution-phase dye concentrations at the initial time, time t, and equilibrium, respectively. V is the volume of the solution (L) and m is the mass of the AN waste adsorbent (g).

2.4. Mechanisms of RB5 and BBY adsorption using isotherms and fit of kinetics models

The mechanisms of the adsorption of RB5 and BBY on the AN waste adsorbent were explored by analyzing the different isotherms and fit of the kinetics models to the equilibrium adsorption data. The experimental data were collected at initial dye concentrations in the range of 10–500 mg/L. The conditions of the batch reactor were set as follows: solution pH 5.0; temperature, 30°C; adsorbent dose, 1.0 g; agitation speed, 220 rpm; and equilibrium times of the two dyes studied. The Langmuir, Freundlich, and Dubinin–Radushkevich (D–R) isotherm models were applied. The corresponding correlations and constants of the model plots were calculated. The AN adsorption data for both the dyes were collected at initial dye concentrations of 50 mg/L at different time intervals, while the remaining aforementioned process conditions were maintained constant. All batch experiments were performed thrice or at least in duplicate and their average values are presented in Figs. 4–6 for corresponding samples. Additional analyses were conducted whenever two measurements differed by more than 5%. The one-way analysis of variance (ANOVA) was performed with the least significant difference of means at $p = 0.01$.

3. Results and discussion

3.1. Surface morphology and elemental analyses of AN adsorbent

The SEM micrographs of the AN adsorbent were captured at magnifications of ×250, ×500, and ×1,000 (Figs. 2a–c). These revealed a porous surface morphology, which renders AN a suitable choice for the adsorption of RB5 and BBY dyes. Energy-dispersive X-ray analysis was conducted to analyze the elemental composition of the AN adsorbent (Fig. 2d). The results, on a weight basis, demonstrated that AN was mainly composed of carbon (56.26%) and oxygen (43.45%), followed by potassium (0.15%), and calcium (0.14%).

3.2. Surface chemistry of AN adsorbent

The FTIR analysis of the AN adsorbent prior to the adsorption of the RB5 and BBY dyes revealed the presence of spectral peaks at 931, 1,060; 1,159; 1,593; and 3,383 cm^{-1}, which corresponded to the N–H (amines), C–N stretch (aliphatic amines), C–N stretch (aromatics), N–H (amides), and O–H stretch (alcohols and phenols), respectively. The presence of these functional groups on the surface of the AN adsorbent has been reported previously [30]. The surface chemistry of the AN adsorbent after the loading of RB5 was not analyzed because mass transfer gradient and intraparticle diffusion were observed as the main driving forces of the transfer of RB5 from the liquid phase (aqueous solution) to the solid phase of the AN adsorbent. In the case of BBY, the mechanism of dye adsorption on the surface of the AN adsorbent was characterized by a monolayer adsorption, high mean free energy (D–R model), and chemisorption. Therefore, the AN adsorbent was analyzed for changes in the surface functional groups after the loading of BBY (Fig. 3). The FTIR spectra revealed peaks at 1,028; 1,210; 1,608; 1,710; 2,980; and 3,306 cm^{-1}, which were assigned to the C–N stretch (aliphatic amines), C–O stretch (carbonyls), N–H bending (amides), C=O stretch (aldehydes), C–H stretch (alkanes), and O–H stretch (alcohols), respectively. The appearance of IR peaks corresponding to the carbonyl, aldehyde, and alkane groups after the adsorption of BBY confirmed the chemical interference between the dye molecules and adsorbent surface.

3.3. Influences of process variables on batch reactor adsorption of RB5 and BBY dyes

3.3.1. Contact time

The influence of contact time on the adsorption capacities (q_t, mg/g) of the AN adsorbent for the RB5 and BBY dyes is shown in Fig. 4. The results clearly reflect the variation in q_t of the AN adsorbent for the dyes studied. In the case of RB5, q_t increased sharply during 10–120 min mainly owing to the abundant presence of unused active sites on the adsorbent surface. Thereafter, there was no increase in the adsorption of the dye, even when the contact time was increased to 160 min owing to the decreased number of active sites available for adsorption on the adsorbent surface.

The maximum adsorption capacity of the AN adsorbent for the RB5 dye was determined to be 38.38 mg/g in 120 min. This value is 71% higher than that reported for the

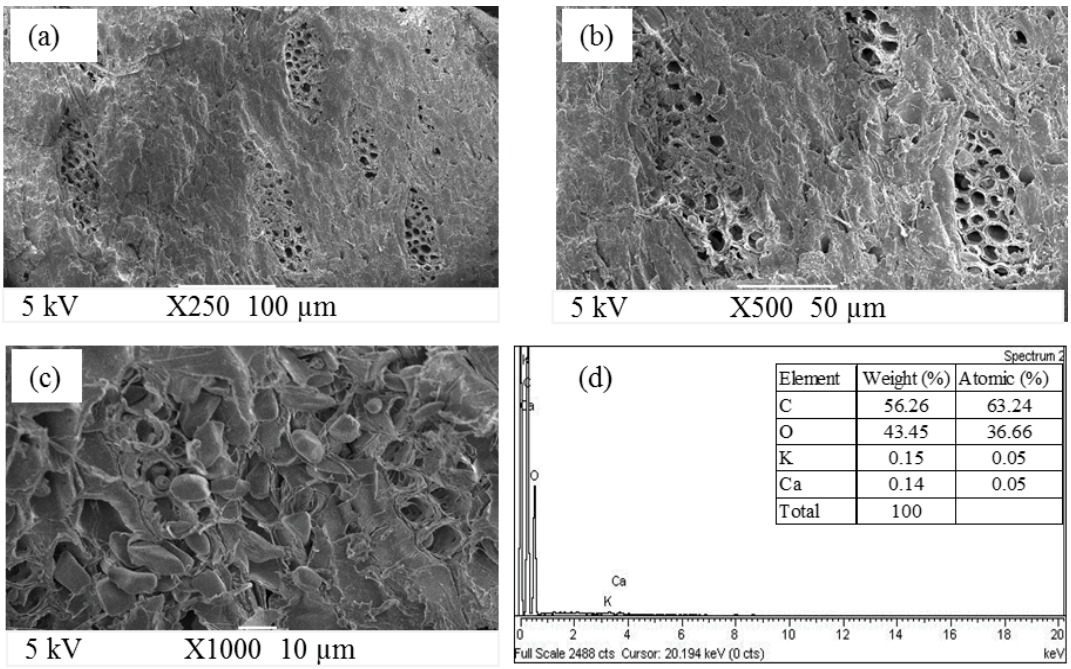

Fig. 2. SEM micrographs at various magnifications (a–c) and EDX analysis (d).

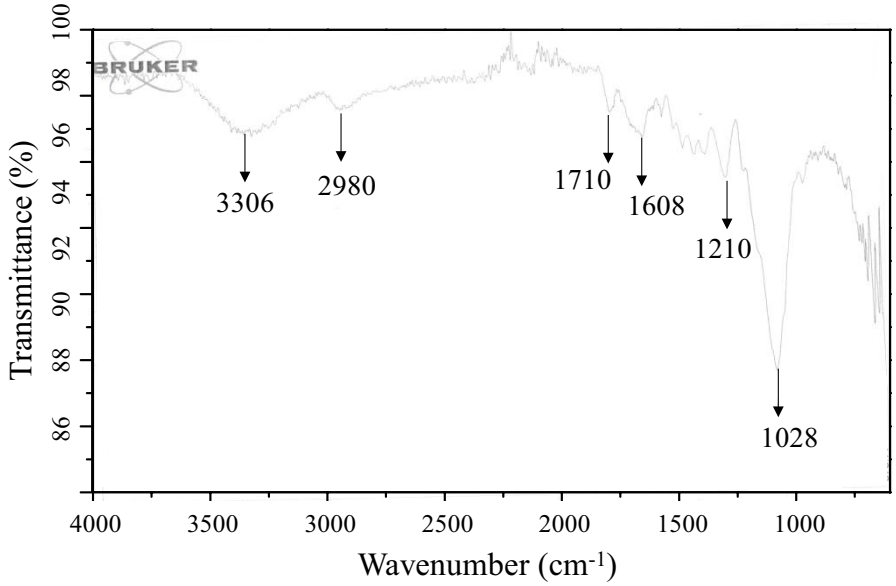

Fig. 3. FTIR spectra of AN adsorbent after adsorption of BBY.

treatment of the same dye using mandarin peels [31], and further compared with previous studies (Table 1). Similarly, for the BBY dye, the AN adsorbent showed a high adsorption capacity of 39.31 mg/g in 30 min, which almost remained constant or increased very insignificantly (p = 0.01) with time (Fig. 5). Therefore, this adsorbent can be deemed a potential choice for the large-scale application of the sequestration of dyes because of its good adsorption capacity and economic viability. The contact time durations of 120 and 30 min were marked as the equilibrium times for the adsorption of the RB5 and BBY dyes, respectively, by the AN adsorbent. Therefore, the remainder of the batch experiments for RB5 and BBY were conducted at 120 and 30 min, respectively.

3.3.2. Initial dye concentration

The initial solution concentrations of the RB5 and BBY dyes significantly influence the assessment of the batch reactor performance for their removal by the AN adsorbent (Fig. 5). The reactor performance was investigated at initial dye concentrations in the range 25–180 mg/L. The adsorption capacity of the AN adsorbent increased from 7.37 to

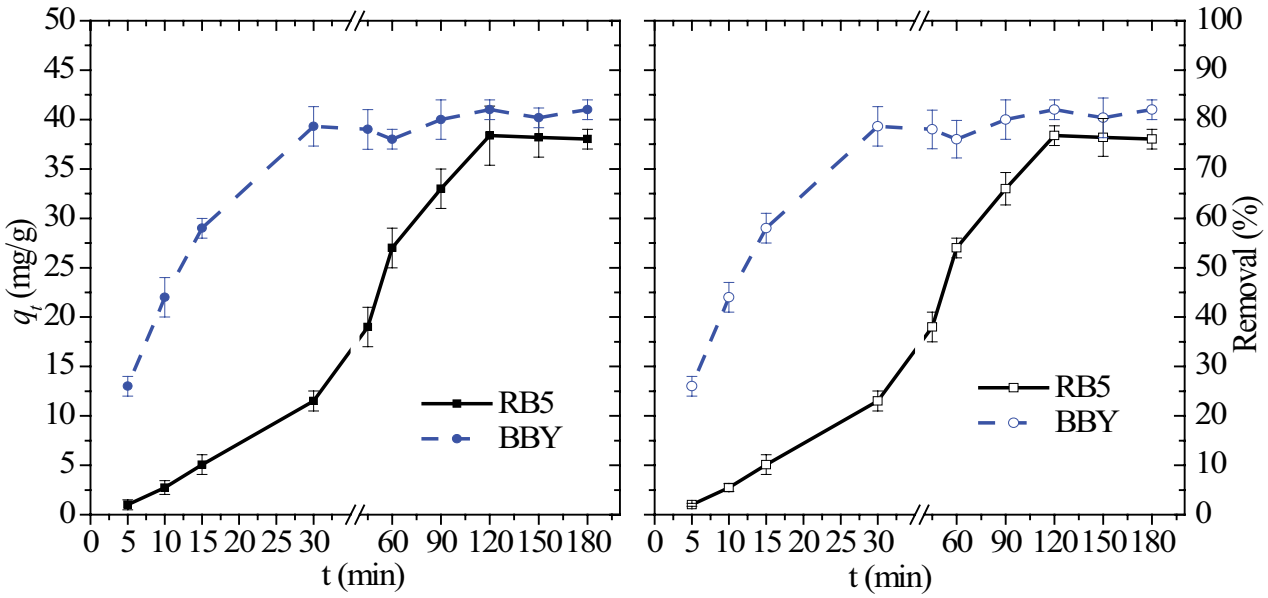

Fig. 4. Influence of contact time on adsorption performance of batch reactor for RB5 and BBY dyes.

Table 1
Comparison of the AN adsorbent with other adsorbents for maximum adsorption capacities

Adsorbent	Dyes	Experimental conditions	Adsorption capacity, mg/g	Reference
Modified pea peels	Bismarck Brown-R	pH-10, temperature-35°C, contact time-60 min	5.37	[32]
Peanut hull	Reactive Black-5	pH-0.5, temperature-60°C, contact time-420 min	55.5	[33]
Banana peel powder	Reactive Black-5	pH-3, temperature-45°C, contact time-180 min	49.2	[34]
Walnut wood AC	Reactive Black-5	pH- 5, temperature-24°C, contact time-405 min	9.85	[35]
Pumice rock	Reactive Black-5	pH-5, temperature-24°C, contact time-120 min	4.65	[35]
Non-catalytically pine waste biochar	Reactive Black-5	pH-9.6, contact time-40 min	4.37	[36]
MWCNT	Bismarck Brown R	pH-5, temperature-25°C, contact time-10 min	30.6	[37]
AN timber waste	Reactive Black-5	pH-2, temperature-30°C, contact time-120 min	38.38	This study
AN timber waste	Bismarck Brown-Y	pH 2, temperature-30°C, contact time-30 min	39.31	This study

104.79 mg/g for the RB5 dye and from 19.65 to 113.48 mg/g for the BBY dye as the dye concentration in the solution increased. This result suggested that the effective mass transfers of the RB5 and BBY dyes from the solution phase to the adsorbent surface were controlled by their respective concentration gradients. Moreover, the higher adsorption of BBY by the AN adsorbent, i.e., 19.65 mg/g, compared with that of RB5, that is, 7.37 mg/g, at an initial dye concentration of 25 mg/L in both cases, revealed that electrostatic interactions were operative.

3.3.3. pH

The adsorbent surface, dye solubility, and adsorption capacity are influenced significantly by variations in the solution pH. The influence of solution pH in the range 2–10 on the adsorption processes of the RB5 and BBY dyes was investigated and the results are shown in Fig. 6. Constant values of the dose of AN adsorbent (1.0 g), initial dye concentrations (50 mg/L), and contact time (120 min) were used for the batch experiments to optimize the solution pH. The maximum adsorption capacities of the AN adsorbent for the RB5 and BBY dyes at a pH of 2 were 19 and 40.07 mg/g, respectively. The behavior of the AN adsorbent under only acidic solution condition was studied by determining the pH at point of zero charge (pHpzc). Titration with 0.1 M KNO_3 solution was performed with initial pH range of 2–7 and the pHpzc was found to be nearly 2.5.

The low pH may have influenced the adsorbent surface by creating more positive sites, which can attract the negatively charged dye molecules. This reflects the different chemical interferences of the RB5 and BBY dyes under similar reaction conditions at the solid–liquid interface. Contrary to this, the adsorption capacity of the AN adsorbent for RB5 decreased to 11.25 mg/g at a pH of 5 and above, while that for BBY decreased to 0.4 mg/g at a

pH of 8. These results illustrate the variable behaviors of the AN adsorbent and the two dyes. The decreased adsorption capacities of the AN adsorbent for both the dyes can be attributed to the competition between the hydroxyl ions and negatively charged dye ions for the active adsorption sites on the adsorbent surface.

3.4. Kinetics modeling

Kinetics models such as pseudo-first-order, pseudo-second-order and intra-particle diffusion models were applied to analyze the rates of RB5 and BBY uptake by the AN adsorbent. The corresponding coefficients of correlations and rate constants of these models were determined.

3.4.1. Pseudo-first-order and pseudo-second-order models

The equations of pseudo-first-order and pseudo-second-order kinetics models [38–41] are given as Eqs. (4) and (5), respectively.

$$q_t = q_e\left(1-\exp\left(-k_1\cdot t\right)\right) \tag{4}$$

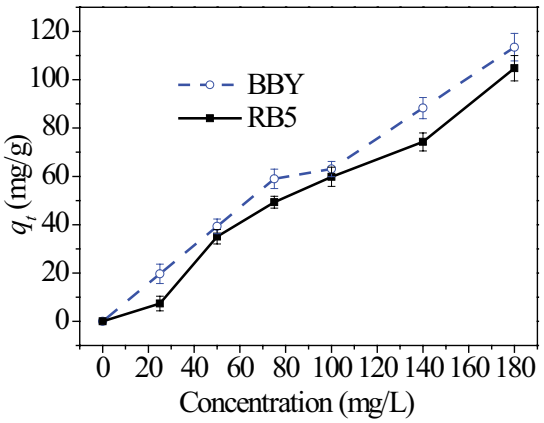

Fig. 5. Influence of initial concentrations of RB5 and BBY on removal performance of AN in batch reactor.

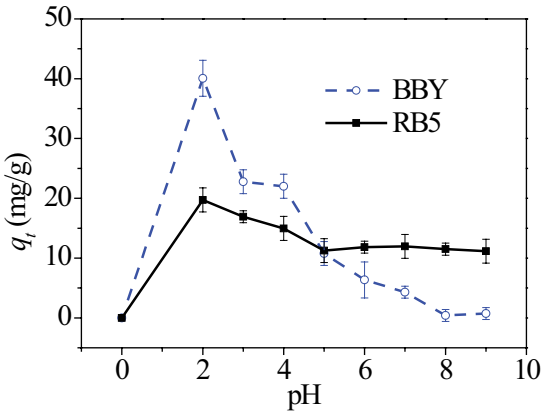

Fig. 6. Influence of pH on removal performance of AN adsorbent for RB5 and BBY dyes in batch reactor.

$$q_t = \frac{\left(q_e^2 k_2\cdot t\right)}{\left(q_e k_2\cdot t+1\right)} \tag{5}$$

Here q_t is the amount of dye adsorbed at time t (min). k_1 (1/min) and k_2 (g/mg/min) are the pseudo-first-order and pseudo-second-order rate constants, respectively, calculated from the respective nonlinear plots. The adsorption of BBY on the AN adsorbent was best described by the pseudo-second-order model with an R^2 value of 0.94 and 0.96 for BBY and RB5, respectively, which confirmed that chemisorption of the dye on the adsorbent surface as the rate-limiting step (Fig. 7, Table 2). This result is similar to the previous kinetic results obtained for various adsorbent–adsorbate systems [42–44]. Chemisorption involves the exchange or sharing of electrons between the adsorbent and adsorbate. However, the adsorption of both dyes on the AN adsorbent revealed a poor fit to the pseudo-first-order kinetics model (except for the initial contact time of about 30 min), which suggested the involvement of some other physical force enabling a fit to the Freundlich isotherm model. Moreover, a higher initial adsorption rate (h) of the AN adsorbent was observed for BBY (5.12 mg/g/min) than that for the RB5 dye (0.628 mg/g/min). The higher value of h indicated the preference of the AN adsorbent for the BBY dye than for RB5.

3.4.2. Intra-particle diffusion kinetics

This model can be used to explore the contaminant adsorption pathway and the driving force of adsorption [45–48]. During the adsorption of dyes on the AN adsorbent, q_t should change linearly with the square root of time (Eq. (6)).

$$q_t = K_{ip}t^{\frac{1}{2}} + C_i \tag{6}$$

Here q_t (mg/g) is the adsorption capacity at time t, C_i is the boundary-layer thickness, and K_{ip} (mg/g/min$^{0.5}$) is the

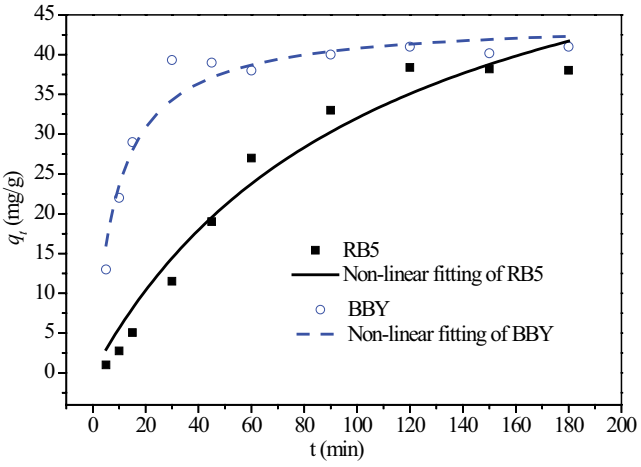

Fig. 7. Pseudo-second-order model fit to adsorption of BBY and RB5 on AN.

Table 2
Constants in pseudo-first-order, pseudo-second-order, and intra-particle diffusion models at 50 mg/L of both dyes

Kinetic model	Parameter	BBY	RB5
Pseudo-first-order	$q_{e,exp}$ (mg/g)	39.3	35.02
	$q_{e,cal}$ (mg/g)	40.35	45.3
	k_1 (1/min)	0.08	0.01
	R^2	0.98	0.97
Pseudo-second-order	$q_{e,cal}$ (mg/g)	44.37	66.98
	k_2 (g/mg/min)	0.0026	0.00014
	h (mg/g/min)	5.12	0.628
	R^2	0.94	0.96
Intra-particle diffusion	K_{ip} (mg/g/min$^{0.5}$)	1.99	3.85
	C (mg/g)	19.3	–7.6
	R^2	0.659	0.94

intra-particle diffusion rate constant. K_{ip} and C_i were calculated from the nonlinear fitting of the curve (q_t vs. t), as shown in Fig. 8.

Fig. 8 shows that the plot for BBY adsorption is non-linear over the entire time range with R^2 = 0.659. The fitted curve of the plot did not pass through the origin, which could be attributed to the variation in mass transfer in the initial and final stages of the adsorption of BBY on AN. This revealed that intra-particle diffusion was not the sole rate-controlling step during the process of adsorption and that, initially, surface adsorption (chemisorption) occurred for this particular dye. In this manner, BBY moved rapidly from the concentrated solution to the primary pores of the AN adsorbent, as shown in the SEM photographs. Chemical interactions occurred between the dye molecules and the functional groups present on the adsorbent surface. However, in the case of RB5 adsorption, the fit of this model was found to be adequate with R^2 = 0.94 and the curve passed through the origin (Fig. 8, Table 2). This result confirmed that intra-particle diffusion and mass transfer gradient were the forces driving the adsorption of RB5 dye on the AN adsorbent.

3.5. Mechanisms of RB5 and BBY adsorption on surface of AN adsorbent

Several operating parameters can affect the rate and adsorption of dye molecules on the surface of the adsorbent. Therefore, multiple mathematical isotherms need to be applied to understand the unabridged phenomenon and driving forces of adsorption. In this study, the Langmuir, Freundlich, and D–R isotherm models were applied to elucidate the mechanisms of adsorption of RB5 and BBY on the surface of the AN adsorbent.

3.5.1. Langmuir isotherm

The Langmuir model assumes monolayer adsorption and energetically homogeneous active sites with no lateral interaction between the adsorbed species [49–52]. The RB5 and BBY adsorption data of the AN adsorbent were analyzed using the nonlinear mathematical expression of the Langmuir isotherm (Eq. (7)).

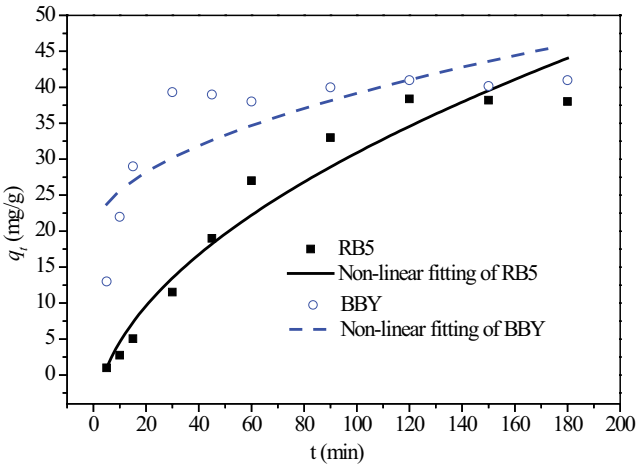

Fig. 8. Intra-particle diffusion model fit to adsorption of BBY and RB5 on AN.

$$q_e = \frac{\left(q_{max} K_L C_e\right)}{\left(1 + K_L C_e\right)} \tag{7}$$

Here C_e is the equilibrium concentration (mg/L), q_e is the amount of dye adsorbed at equilibrium, q_{max} is the maximum adsorption capacity (mg/g), and K_L (L/mg) is the Langmuir constant. The constant for each dye was calculated from the nonlinear fitting of the curve, as shown in Fig. 9a. This model adequately described the adsorption of BBY on the AN adsorbent with a coefficient of determination R^2 = 0.99 compared with the adsorption of RB5 with an R^2 value of 0.97 (Fig. 9a). The value of K_L characterizes the adsorption affinity between the adsorbate and adsorbent. The value of K_L was found to be 0.02 L/mg for both the dyes (Table 3), which revealed the strong attraction of BBY and RB5 toward the AN adsorbent. On the basis of the R^2 values, the goodness-of-fit of the data reflected the monolayer adsorption of

Table 3
Calculated parameters of Langmuir, Freundlich, and D–R isotherm models at 180 mg/L of both dyes

Isotherm model	Parameters	BBY	RB5
Langmuir	$q_{e,exp}$ (mg/g)	113.48	104.78
	q_{max} (mg/g)	210	137.92
	K_L (L/mg)	0.016	0.0234
	R_L	0.26	0.19
	R^2	0.99	0.97
Freundlich	q_m (mg/g)	148.9	105.2
	K_F ((mg/g)(L/mg)$^{1/n}$)	15.39	17.1
	$1/n$	0.437	0.35
	R^2	0.97	0.90
Dubinin–Radushkevich	q_m (mol/g)	164	111
	β (mol/kJ)^2)	0.0024	0.002
	E (kJ/mol)	14.43	15.81
	R^2	0.80	0.86

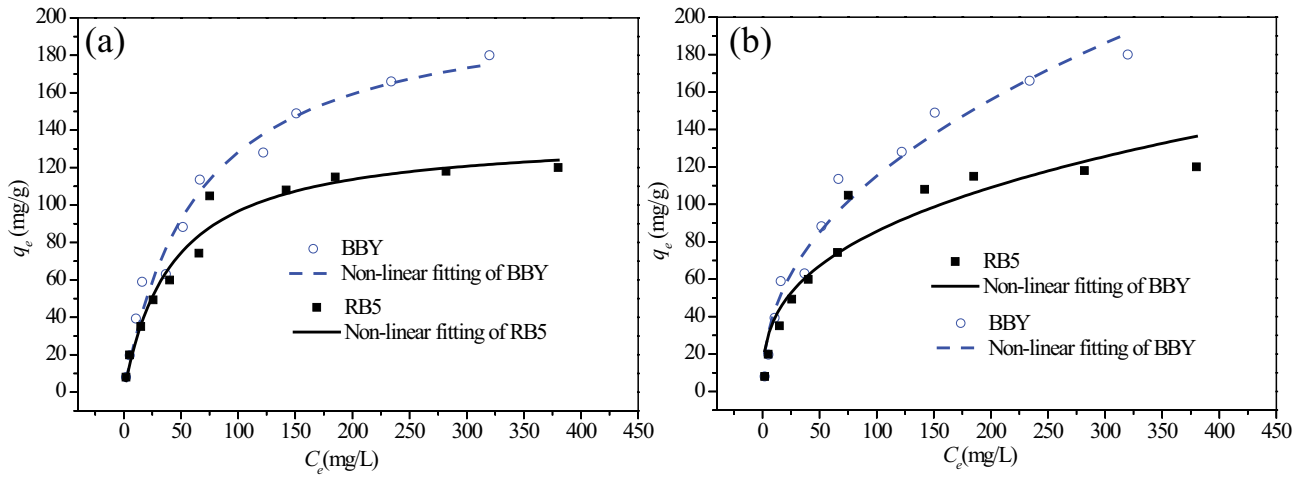

Fig. 9. Langmuir (a) and Freundlich (b) isotherm model fitness to the adsorption data for the RB5 and BBY dyes on the AN adsorbent.

the BBY dye on the surface of the AN adsorbent. In the literature, similar isotherm model-fitting has been obtained for the adsorption isotherms of various dyes [53–55].

The separation factor/dimensionless constant (R_L = 1/(1 + $K_L C_0$)) indicates if the process is linear (R_L = 1), unfavorable (R_L > 1), irreversible (R_L = 0), and or favorable (0 < R_L < 1). The values of R_L for the adsorption of RB5 and BBY on the AN adsorbent were 0.19 and 0.26 (Table 3), respectively, which indicated that this process was favored.

3.5.2. Freundlich isotherm

The Freundlich model (Eq. (8)) provides physical insights into the adsorption phenomenon [56–58].

$$q_e = K_F C_e^{1/n} \tag{8}$$

Here K_F ((mg/g)(L/mg)$^{1/n}$) and 1/n are the Freundlich constants, which indicate the adsorption capacity and adsorption intensity, respectively, and can be calculated from the plot of q_e vs. c_e. This model exhibited a better fit to the BBY adsorption data with R^2 value of 0.97 (Fig. 9b) than to the RB5 adsorption data with R^2 value of 0.90. This shows that the adsorption of BBY is primarily controlled by physical forces and that the adsorbed molecules form a multilayer on the surface of the AN adsorbent. The magnitude of 1/n reveals the favorability/non-favorability of the studied AN adsorbent for toward the adsorption of the RB5 and BBY dyes. The values of 1/n for RB5 and BBY were 0.35 and 0.437, respectively, which are less than 1.0 (Table 3), and imply the favorability of the adsorption of these dyes on the AN adsorbent.

3.5.3. Dubinin–Radushkevich isotherm

The D–R model (Eq. (9)) assumes that adsorption takes place on a non-homogenous surface with Gaussian energy distribution and in the micropores following in accordance with a pore-filling mechanism [59,60]. This model can discriminate between the physical and chemical natures of the adsorption process. The D–R isotherm can be expressed as:

$$q_e = q_{DR} \exp\left(-\beta\varepsilon^2\right) \tag{9}$$

The D–R isotherm showed a comparatively poorer fit to the adsorption data of BBY than to those of the RB5 adsorption data, with R^2 values of 0.80 and 0.86, respectively (Fig. 10). The Polanyi potential is presented by Eq. (10).

$$\varepsilon = RT \ln\left(1 + \frac{1}{C_e}\right) \tag{10}$$

Here R is the universal gas constant (8.314 J/mol/K) and T is the temperature (K). The free energy per molecule (E) of RB5 in the sorption space for movement to infinity can be determined from Eq. (11).

$$E = \frac{1}{\sqrt{2\beta}} \tag{11}$$

A high value of E (>8 kJ/mol) is typically associated with chemisorption. In this study, the E values for the adsorption of RB5 and BBY dyes on the surface of the AN adsorbent were found to be 15.81 and 14.43 kJ/mol, respectively (Table 3). This result suggests that the chemisorption of RB5 on the AN adsorbent is stronger than that of BBY and this additionally indicates the involvement of the ion exchange mechanism between the adsorbate and the functional groups present on the adsorbent surface of the AN adsorbent.

The experimental data of the adsorption of BBY on the AN adsorbent best fits the isotherm models in the following order: Langmuir (0.99) > Freundlich (0.97) > D–R (0.80). Similarly, the adsorption of RB5 followed a similar order to fit the isotherm models with slight variation in the corresponding R^2 values, as shown in Table 3.

3.6. Regeneration of AN adsorbent

Desorption experiments were conducted in batch mode to check the uptake adsorption capacity and the possibility

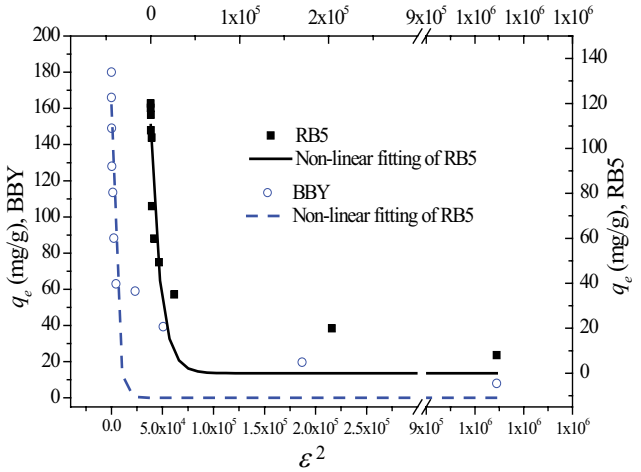

Fig. 10. Dubinin–Radushkevich (D–R) isotherm model fitness to adsorption data of BBY and RB5.

of reusability and regeneration of the AN adsorbent. RB5 and BBY dyes were strongly bonded to AN surface therefore, 0.1 M HCl was used as eluent along with some heat treatment for 24 h. It was noticed that after every desorption cycle, the uptake adsorption capacity of both RB5 and BBY dyes onto AN adsorbent decreased slowly and adsorbent exhausted after three desorption cycles.

4. Conclusions

In this work, the batch adsorption conditions of RB5 and BBY dyes on AN adsorbent were optimized. The maximum adsorption capacities of the AN adsorbent for RB5 and BBY were observed at contact times of 120 and 30 min, respectively, pH of 2, and initial dye concentration of 180 mg/L. The equilibria between the dyes in the solution phase and on the surface of the AN adsorbent were attained at 120 and 30 min for RB5 and BBY, respectively. The adsorption of both the dyes decreased with an increase in pH. The AN adsorbent exhibited a dual behavior for the adsorption of the two different dyes. The adsorption of BBY was best described by the Langmuir isotherm and pseudo-second-order kinetic models. The isotherm model fit displayed single-layer adsorption of BBY on the adsorbent surface and chemisorption was the dominant operative force with an *E* value (D–R model) of 14.43 kJ/mol. This was verified by the appearance of spectral peaks corresponding to the carbonyl, aldehyde, and alkane groups after the adsorption of BBY on the adsorbent. On the other hand, intra-particle diffusion driven by a mass transfer gradient was primarily responsible for the adsorption of RB5 on the surface of the AN adsorbent.

Acknowledgments

The project was financially supported by King Saud University, Vice Deanship of Research Chairs. The authors would also like to thank the Research Support and Services Unit (RSSU) at King Saud University for its editing services.

References

[1] T. Robinson, G. McMullan, R. Marchant, P. Nigam, Remediation of dyes in textile effluent: a critical review on current treatment technologies with a proposed alternative, Bioresour. Technol., 77 (2001) 247–255.
[2] A.K. Jain, V.K. Gupta, A. Bhatnagar, Suhas, A comparative study of adsorbents prepared from industrial wastes for removal of dyes, Sep. Sci. Technol., 38 (2003) 463–481.
[3] P.C. Vandevivere, R. Bianchi, W. Verstraete, Review: treatment and reuse of wastewater from the textile wet-processing industry: review of emerging technologies, J. Chem. Technol. Biotechnol., 72 (1998) 289–302.
[4] M.M. Naim, Y.M. El Abd, Removal and recovery of dyestuffs from dyeing wastewaters, Sep. Purif. Rev., 31 (2002) 171–228.
[5] R. Kant, Textile dyeing industry an environmental hazard, Nat. Sci., 4 (2012) 22–26.
[6] N. Mathur, P. Bhatnagar, P. Bakre, Assessing mutagenicity of textile dyes from Pali (Rajasthan) using Ames bioassay, Appl. Ecol. Environ. Res., 4 (2006) 111–118.
[7] K. Mortelmans, E. Zeiger, The Ames *Salmonella*/microsome mutagenicity assay, Mutat. Res. Mol. Mech. Mutagen., 455 (2000) 29–60.
[8] S.W. Geis, K.L. Fleming, E.T. Korthals, G. Searle, L. Reynolds, D.A. Karner, Modifications to the algal growth inhibition test for use as a regulatory assay, Environ. Toxicol. Chem., 19 (2000) 36–41.
[9] K. Hunger, R. Hamprecht, P. Miederer, C. Heid, A. Engel, K. Kunde, W. Mennicke, J. Griffiths, Dye Classes for Principal Applications, K. Hunger, Ed., Industrial Dyes, Wiley-VCH Verlag GmbH & Co. KGaA, Weinheim, Germany, 2002, pp. 113–338.
[10] R.M. Christie, Environmental Aspects of Textile Dyeing, Elsevier, Woodhead Publishing Ltd., Cambridge, 2007.
[11] R. Li, B. Gao, K. Guo, Q. Yue, H. Zheng, Y. Wang, Effects of papermaking sludge-based polymer on coagulation behavior in the disperse and reactive dyes wastewater treatment, Bioresour. Technol., 240 (2017) 59–67.
[12] A.Y. Zahrim, Z.D. Dexter, C.G. Joseph, N. Hilal, Effective coagulation-flocculation treatment of highly polluted palm oil mill biogas plant wastewater using dual coagulants: decolourisation, kinetics and phytotoxicity studies, J. Water Process Eng., 16 (2017) 258–269.
[13] A. Turcanu, T. Bechtold, Cathodic decolourisation of reactive dyes in model effluents released from textile dyeing, J. Cleaner Prod., 142 (2017) 1397–1405.
[14] S. Shekoohiyan, G. Moussavi, S. Mojab, A. Alahabadi, Adsorption of the reactive azo dyes onto NH_4Cl-induced activated carbon, Environ. Health Eng. Manage., 3 (2016) 1–7.
[15] M.T. Amin, A.A. Alazba, M. Shafiq, Adsorptive removal of reactive black 5 from wastewater using bentonite clay: isotherms, kinetics and thermodynamics, Sustainability, 7 (2015) 15302–15318.
[16] J. Lin, W. Ye, H. Zeng, H. Yang, J. Shen, S. Darvishmanesh, P. Luis, A. Sotto, B. Van der Bruggen, Fractionation of direct dyes and salts in aqueous solution using loose nanofiltration membranes, J. Membr. Sci., 477 (2015) 183–193.
[17] N. Askari, M. Farhadian, A. Razmjou, H. Hashtroodi, Nanofiltration performance in the removal of dye from binary mixtures containing anthraquinone dyes, Desal. Water Treat., 57 (2016) 18194–18201.
[18] L. Škodič, S. Vajnhandl, J. Volmajer Valh, T. Željko, B. Vončina, A. Lobnik, Comparative study of reactive dyes oxidation by H_2O_2/UV, H_2O_2/UV/Fe^{2+} and H_2O_2/UV/Fe^0 processes, Ozone Sci. Eng., 39 (2017) 14–23.
[19] Z. Zhu, M. Zhang, F. Liu, C. Shuang, C. Zhu, Y. Zhang, A. Li, Effect of polymeric matrix on the adsorption of reactive dye by anion-exchange resins, J. Taiwan Inst. Chem. Eng., 62 (2016) 98–103.
[20] G.G. Lenzi, R.F. Evangelista, E.R. Duarte, L.M.S. Colpini, A.C. Fornari, R. Menechini Neto, L.M.M. Jorge, O.A.A. Santos, Photocatalytic degradation of textile reactive dye using artificial neural network modeling approach, Desal. Water Treat., 57 (2016) 14132–14144.

[21] C. Zaharia, D. Suteu, A. Muresan, R. Muresan, A. Popescu, Textile wastewater treatment by homogenous oxidation with hydrogen peroxide, Environ. Eng. Manage. J., 8 (2009) 1359–1369.
[22] K.K. Krishnani, X. Meng, C. Christodoulatos, V.M. Boddu, Biosorption mechanism of nine different heavy metals onto biomatrix from rice husk, J. Hazard. Mater., 153 (2008) 1222–1234.
[23] N. Atar, A. Olgun, S. Wang, S. Liu, Adsorption of anionic dyes on boron industry waste in single and binary solutions using batch and fixed-bed systems, J. Chem. Eng. Data, 56 (2011) 508–516.
[24] V.K. Garg, M. Amita, R. Kumar, R. Gupta, Basic dye (methylene blue) removal from simulated wastewater by adsorption using Indian Rosewood sawdust: a timber industry waste, Dyes Pigm., 63 (2004) 243–250.
[25] A. Bhatnagar, A.K. Jain, A comparative adsorption study with different industrial wastes as adsorbents for the removal of cationic dyes from water, J. Colloid Interface Sci., 281 (2005) 49–55.
[26] M.A.M. Salleh, D.K. Mahmoud, W.A.W.A. Karim, A. Idris, Cationic and anionic dye adsorption by agricultural solid wastes: a comprehensive review, Desalination, 280 (2011) 1–13.
[27] S. Senthilkumaar, P. Kalaamani, K. Porkodi, P.R. Varadarajan, C.V. Subburaam, Adsorption of dissolved reactive red dye from aqueous phase onto activated carbon prepared from agricultural waste, Bioresour. Technol., 97 (2006) 1618–1625.
[28] N.K. Amin, Removal of reactive dye from aqueous solutions by adsorption onto activated carbons prepared from sugarcane bagasse pith, Desalination, 223 (2008) 152–161.
[29] M.A. Tahir, H.N. Bhatti, M. Iqbal, Solar Red and Brittle Blue direct dyes adsorption onto *Eucalyptus angophoroides* bark: equilibrium, kinetics and thermodynamic studies, J. Environ. Chem. Eng., 4 (2016) 2431–2439.
[30] M.T. Amin, A.A. Alazba, M. Shafiq, Nonspontaneous and multilayer adsorption of malachite green dye by *Acacia nilotica* waste with dominance of physisorption, Water Sci. Technol., 76 (2017) 1805–1815.
[31] J.F. Osma, V. Saravia, J.L. Toca-Herrera, S.R. Couto, Sunflower seed shells: a novel and effective low-cost adsorbent for the removal of the diazo dye Reactive Black 5 from aqueous solutions, J. Hazard. Mater., 147 (2007) 900–905.
[32] T.A. Khan, R. Rahman, E.A. Khan, Decolorization of bismarck brown R and crystal violet in liquid phase using modified pea peels: non-linear isotherm and kinetics modeling, Model. Earth Syst. Environ., 2 (2016) 141.
[33] M.Ş. Tanyildizi, Modeling of adsorption isotherms and kinetics of reactive dye from aqueous solution by peanut hull, Chem. Eng. J., 168 (2011) 1234–1240.
[34] V.S. Munagapati, V. Yarramuthi, Y. Kim, K.M. Lee, D.-S. Kim, Removal of anionic dyes (Reactive Black 5 and Congo Red) from aqueous solutions using banana peel powder as an adsorbent, Ecotoxicol. Environ. Saf., 148 (2018) 601–607.
[35] B. Heibati, S. Rodriguez-Couto, A. Amrane, M. Rafatullah, A. Hawari, M.A. Al-Ghouti, Uptake of Reactive Black 5 by pumice and walnut activated carbon: chemistry and adsorption mechanisms, J. Ind. Eng. Chem., 20 (2014) 2939–2947.
[36] A. Khan, A. Rashid, R. Younas, Adsorption of reactive black-5 by pine needles biochar produced via catalytic and non-catalytic pyrolysis, Arabian J. Sci. Eng., 40 (2015) 1269–1278.
[37] A.M. Kamil, F.H. Abdalrazak, A.F. Halbus, F.H. Hussein, Adsorption of bismarck brown R dye onto multiwall carbon nanotubes, J. Environ. Anal. Chem., 1 (2014) 104.
[38] A. Bhatnagar, A.K. Minocha, M. Sillanpää, Adsorptive removal of cobalt from aqueous solution by utilizing lemon peel as biosorbent, Biochem. Eng. J., 48 (2010) 181–186.
[39] Y.S. Ho, G. McKay, Pseudo-second order model for sorption processes, Process Biochem., 34 (1999) 451–465.
[40] A. Hamzah, W.N.W.M. Arifin, K.S. Khoo, L.J. Lee, S.B. Sarmani, Screening of biosorption bacteria tolerance towards copper and cadmium from oil sludge pond, J. Radioanal. Nucl. Chem., 281 (2009) 295–298.
[41] M.A. Hubbe, S. Azizian, S. Douven, Implications of apparent pseudo-second-order adsorption kinetics onto cellulosic materials: a review, BioResources, 14 (2019) 7582–7626.
[42] O. Duman, C. Özcan, T. Gürkan Polat, S. Tunç, Carbon nanotube-based magnetic and non-magnetic adsorbents for the high-efficiency removal of diquat dibromide herbicide from water: OMWCNT, OMWCNT-Fe_3O_4 and OMWCNT-κ-carrageenan-Fe_3O_4 nanocomposites, Environ. Pollut., 244 (2019) 723–732.
[43] O. Duman, E. Ayranci, Adsorptive removal of cationic surfactants from aqueous solutions onto high-area activated carbon cloth monitored by in situ UV spectroscopy, J. Hazard. Mater., 174 (2010) 359–367.
[44] E. Ayranci, O. Duman, Structural effects on the interactions of benzene and naphthalene sulfonates with activated carbon cloth during adsorption from aqueous solutions, Chem. Eng. J., 156 (2010) 70–76.
[45] A.R. Kul, H. Koyuncu, Adsorption of Pb(II) ions from aqueous solution by native and activated bentonite: kinetic, equilibrium and thermodynamic study, J. Hazard. Mater., 179 (2010) 332–339.
[46] S.K. Srivastava, R. Tyagi, N. Pant, Adsorption of heavy metal ions on carbonaceous material developed from the waste slurry generated in local fertilizer plants, Water Res., 23 (1989) 1161–1165.
[47] W.J. Weber, J.C. Morris, Kinetics of adsorption on carbon from solution, J. Sanitary Eng. Div., 89 (1963) 31–60.
[48] E. Demirbas, M. Kobya, E. Senturk, T. Ozkan, Adsorption kinetics for the removal of chromium(VI) from aqueous solutions on the activated carbons prepared from agricultural wastes, Water SA, 30 (2004) 533–539.
[49] I. Langmuir, The Adsorption of gases on plane surface of glass, mica and platinum, J. Am. Chem. Soc., 40 (1918) 1361–1403.
[50] A. Günay, E. Arslankaya, İ. Tosun, Lead removal from aqueous solution by natural and pretreated clinoptilolite: adsorption equilibrium and kinetics, J. Hazard. Mater., 146 (2007) 362–371.
[51] H.N. Tran, S.-J. You, A. Hosseini-Bandegharaei, H.-P. Chao, Mistakes and inconsistencies regarding adsorption of contaminants from aqueous solutions: a critical review, Water Res., 120 (2017) 88–116.
[52] S.O. Lesmana, N. Febriana, F.E. Soetaredjo, J. Sunarso, S. Ismadji, Studies on potential applications of biomass for the separation of heavy metals from water and wastewater, Biochem. Eng. J., 44 (2009) 19–41.
[53] O. Duman, S. Tunç, B.K. Bozoğlan, T.G. Polat, Removal of triphenylmethane and reactive azo dyes from aqueous solution by magnetic carbon nanotube-κ-carrageenan-Fe_3O_4 nanocomposite, J. Alloys Compd., 687 (2016) 370–383.
[54] O. Duman, S. Tunç, T.G. Polat, B.K. Bozoğlan, Synthesis of magnetic oxidized multiwalled carbon nanotube-κ-carrageenan-Fe_3O_4 nanocomposite adsorbent and its application in cationic Methylene Blue dye adsorption, Carbohydr. Polym., 147 (2016) 79–88.
[55] O. Duman, S. Tunç, T.G. Polat, Determination of adsorptive properties of expanded vermiculite for the removal of C I Basic Red 9 from aqueous solution: kinetic, isotherm and thermodynamic studies, Appl. Clay Sci., 109–110 (2015) 22–32.
[56] M.T. Amin, A.A. Alazba, M. Shafiq, Adsorption of copper (Cu^{2+}) from aqueous solution using date palm trunk fibre: isotherms and kinetics, Desal. Water Treat., 57 (2016) 22454–22466.
[57] H.M.F. Freundlich, Over the adsorption in solution, J. Phys. Chem., 57 (1906) 385–471.
[58] M.A.A. Shahmirzadi, S.S. Hosseini, N.R. Tan, Enhancing removal and recovery of magnesium from aqueous solutions by using modified zeolite and bentonite and process optimization, Korean J. Chem. Eng., 33 (2016) 3529–3540.
[59] N. Ayawei, A.T. Ekubo, D. Wankasi, E.D. Dikio, Adsorption of congo red by Ni/Al-CO_3: equilibrium, thermodynamic and kinetic studies, Orient. J. Chem., 31 (2015) 1307–1318.
[60] U. Israel, U.M. Eduok, Biosorption of zinc from aqueous solution using coconut (*Cocos nucifera* L.) coirdust, Arch. Appl. Sci. Res., 4 (2012) 809–819.